J Mater Sci: Mater Electron **(2024) 35:758**

Effect of limited current on ultrarapid densification and giant dielectric properties of flash sintering (La, Ta) co-doped TiO_2 ceramics

Zaizhi Yang[1,2], Xi Wang[3], Liang Zhang[1], Hailing Li[1,*], Hui Zhang[1], and Dong Xu[4,*]

[1] *School of Materials Science and Engineering, Anhui University of Technology, Maanshan 243002, People's Republic of China*
[2] *Department of Materials Engineering, Suqian University, Suqian 223800, People's Republic of China*
[3] *Anhui Dongxun Sealing Technology Co., Ltd, Wuhu 241000, People's Republic of China*
[4] *School of Materials Science and Engineering, Anhui Polytechnic University, Wuhu 241000, People's Republic of China*

Received: 8 February 2024
Accepted: 2 April 2024
Published online: 12 April 2024

ABSTRACT

Flash sintering is considered a promising energy-saving and efficient technology for preparing high-temperature ceramics. The effects of limited current on flash sintering parameters, microstructure, and electrical properties of $(La_{1/2}, Ta_{1/2})_{0.02}Ti_{0.98}O_2$ ceramic were investigated by the XRD, SEM, XPS, and precision impedance analyzer. With limiting current increase, the grain size of flash sintering sample increases gradually, and the relative density increases first and then decreases. The average grain size is about 1 μm, and the highest relative density is 96.9%. Joule heating runaway and oxygen vacancy defect lead to rapid densification of flash sintering La and Ta co-doped TiO_2 ceramics. According to the EPDD model, doped La^{3+} and Ta^{5+} ions increase the concentration of oxygen vacancies and free electrons, lead to local polarization of carriers, and obtain a giant dielectric constant of $\varepsilon' = 7.6 \times 10^4$ and low dielectric loss of $\tan\delta = 0.11$. At high temperature, electrons break free from the constraints of defect clusters and accumulate at the interface, leading to interface polarization due to the IBLC model. The giant dielectric properties originate from the combined effect of EPDD and IBLC model.

1 Introduction

Flash sintering (FS), as a novel type sintering technology with low sintering temperature and short sintering time [1–3], has received widespread attention. With the assistance of applied electric field, ceramics can achieve rapid densification. Since Raj research group [4] first prepared ZnO ceramics at 850 °C and 5 s in 2010, flash sintering has been successfully applied to various ceramic materials, such as ZnO, YSZ, Al_2O_3, Y_2O_3, WC, $SrTiO_3$, $Gd_2Zr_2O_7$, $La_{0.9}Ca_{0.1}CrO_3$, and $(La_{0.2}Nd_{0.2}Sm_{0.2}Eu_{0.2}Gd_{0.2})_2Zr_2O_7$ [3, 5–13]. Obviously, flash sintering has become a hot research topic. The power supply types [10, 14–16], heating equipment [17], sample shape [18, 19], and parameters of flash sintering have been widely studied. The research on

Address correspondence to E-mail: lihl@ahut.edu.cn; frank@shu.edu.cn

https://doi.org/10.1007/s10854-024-12518-3

the mechanism of flash sintering has also made great progress. The theories of Joule thermal effect [20–22], grain boundary overheating effect [23], Frenkel nucleation effect [24], and electrochemical effect [25] have been widely accepted and supported, respectively. However, it is still difficult to explain problems such as rapid densification and luminescence during flash sintering, resulting in great controversy [26–28].

Co-doped TiO_2 ceramics with rutile phase have exhibited excellent giant dielectric properties and become candidate materials for dielectrics due to their high dielectric constant, low dielectric loss, and good dielectric stability in the frequency range of 10–10^6 Hz and temperature range of 80–450 K [29]. The giant dielectric effect of co-doped TiO_2 ceramics has aroused the interest of many researchers and has been verified in the case of various donor ions (Nb^{5+}, Ta^{5+}, Sb^{5+}, W^{6+}, Mo^{6+}) [30–34] and acceptor ions (Ag^{+}, Zn^{2+}, Ca^{2+}, Al^{3+}, Ga^{3+}, Eu^{3+}, Zr^{4+}, Sn^{4+}) [35–42]. Although there has been a large of research on co-doped TiO_2 ceramics, the origin of giant dielectric constant is still unclear and controversial [43]. The giant dielectric theory accepted widely includes electron pinned defect dipole (EPDD) model [29, 44], surface barrier layer capacitor (SBLC) model [45], internal barrier layer capacitor (IBLC) model [39, 46], and polaronic relaxation [47]. However, it is still difficult to reach a consensus on the giant dielectric mechanism. Research on giant dielectric theory of co-doped TiO_2 ceramics is of great significance for the development of electronic functional devices. In addition, co-doped TiO_2 ceramics are usually prepared by conventional solid-state reaction sintering in which sintering temperature exceeds 1400 °C and sintering time is longer than 5 h [31, 44]. High energy consumption and low efficiency lead to coarse grains, deteriorate dielectric properties, and are not conducive to environmental protection.

Co-doped TiO_2 ceramics can be prepared by the flash sintering technology, with lower sintering temperature and shorter sintering time. Peng et al. first prepared (Zr + Ta) co-doped TiO_2 ceramics by flash sintering at 1200 °C and studied the effects of different electric field strengths (500–800 V/cm) on microstructure and giant dielectric properties [48]. Subsequently, other co-doped TiO_2 giant dielectric ceramics were prepared by flash sintering, where the effect of electric field intensity on microstructure and dielectric properties was studied [49–51]. The flash sintering of co-doped TiO_2 has just been preliminarily explored, and the research only focuses on the electric field intensity. Other flash sintering parameters, such as preset limited current, also have an important impact on the densification and properties of ceramics. In this work, La^{3+} and Ta^{5+} co-doped TiO_2 ceramics were successfully prepared by flash sintering. The effects of limited current on the density and microstructure of sintered samples were studied, and the internal principle between sintering parameters and giant dielectric properties was analyzed. With the increase of limited current, the grain size becomes big, dielectric constant decreases, and dielectric loss increases. The giant dielectric properties of co-doped TiO_2 ceramics are attributed to the EPDD model and the IBLC model.

2 Experiment procedure and characterization

Rutile TiO_2 (99.99%), Ta_2O_5 (99.99%), and La_2O_3 (99.99%) from Shanghai Aladdin Co., Ltd were used as the raw materials of experiment. All chemical reagents were weighted according to the stoichiometric ratio of $(La_{1/2}, Ta_{1/2})_{0.02}Ti_{0.98}O_2$ (LTTO) samples after dehumidification for 24 h in a drying oven. Detailed processing of powder reagent was reported previously [50]. The processed powder was uniformly mixed with the 5 wt% polyvinyl alcohol (PVA) and pressed into the green disc with a thickness of about 2.0 mm and a diameter of 7.0 mm by uniaxial pressure at 300 MPa. The green disc was heated at a rate of 2 °C/min to 650 °C for 120 min to remove the PVA binder.

The nickel sheets were used to improve the contact between the sample and the electrode. The green disc was heated at a rate of 10 °C/min to 1100 °C and then kept for 20 min. The direct current (DC) power supply (Sorensen DLM-300, USA) was connected to the green disc to form a closed circuit, and the output voltage is set to maintain a constant electric field strength of 300 V/cm. The initial current parameters were limited from 0.5 to 0.9 A, with an interval of 0.1 A. The limited current stepwise increased at intervals of 0.3 A and was held for 4 min, as shown in Fig. 1. After flash sintering, the sample was cooled to room temperature (25 °C) and labeled as FSC1, FSC2, FSC3, FSC4, and FSC5, respectively.

The blackbody radiation (BBR) model suggested by Raj [20] was used to calculate the surface temperature of the flash sintering sample. Phase structure of LTTO ceramics was determined by the X-ray diffraction (XRD, D8 Advance, Bruker Inc., Germany). According

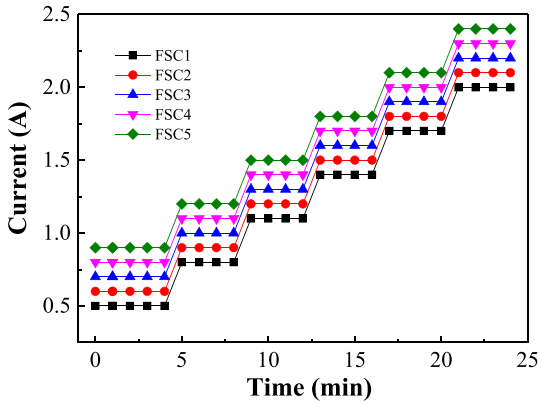

Fig. 1 Preset limited current parameters for flash sintering LTTO samples

to the results of XRD data analysis by Jade software, the theoretical density of the LTTO samples is 4.54 g/cm^3. The bulk density was determined by the Archimedes method [52], and the relative density of flash sintering LTTO samples was expressed as the ratio of bulk density to theoretical density. After fine grinding and polishing of the bottom surface, the sample is subjected to hot corrosion treatment at 1200 °C for 30 min. The microstructure and element distribution of the corroded samples were observed using field-emission scanning electron microscopy (FE-SEM, NANO SEM430, USA) with energy-dispersive X-ray (EDX) spectroscopy produced by FEI Company. The grain size of flash sintering LTTO samples was statistically analyzed using Nano Measurer software. The precision impedance analyzer (Keysight E4990A, USA) was used to measure the impedance spectrum and dielectric properties in the frequency range of 10^2–10^6 Hz at room temperature. The temperature dependence of dielectric performance was measured using a dielectric temperature spectrum testing system (TZDM-RTA-10C, China) in the temperature range of 30–500 °C. The chemical valence states of elements are analyzed by X-ray Photoelectron Spectroscopy (XPS, ESCALAB 250XI, USA). The *E*–*J* curves of flash sintering LTTO samples were measured using a ferroelectric analyzer (2000E, TF Analyzer, Germany).

3 Result and discussion

The voltage, power density, and BBR temperature curves of flash sintering samples are shown in Fig. 2. As can be seen from the voltage curve over time, flash sintering can occur instantly without an incubation period due to the higher electric field intensity. At the moment of flash sintering, the voltage drops sharply, which is attributed to the increase in the conductivity of sample. The local enlarged image at the dashed line is shown in Fig. 2b. During the stable period, the voltage fluctuates slightly with the stepwise increase of the limited current, but the change is not significant. The power density and BBR temperature exhibit the same variation characteristics, which peak at the flash sintering moment and then decrease sharply. As the limited current steps up, the power density and temperature of samples were improved significantly. Moreover, the greater the limited current, the higher the power density and temperature of the flash sintering samples. According to the BBR model, the peak temperature of flash sintering sample can be estimated, as shown in Table 1. FSC5 sample has the highest peak temperature, about 1589 °C.

According to the thermal runaway theory, flash sintering LTTO samples can quickly complete densification, which is attributed to the extremely high heating rate (10^4 °C/min) of Joule heating. However, the peak temperature of the flash sintering sample is only slightly higher than the conventional sintering temperature, and the time is very short, only a few seconds. Therefore, the thermal runaway theory cannot be the only mechanism for the rapid densification of ceramics. At the moment of flash sintering, due to non-equilibrium heating, a large number of vacancies were formed inside the TiO_2 crystal. Vacancy reduces the barrier level of atomic diffusion and also provides a convenient channel for mass diffusion. The atoms inside the crystal are easily diffused into the gaps among the powder, promoting the migration of grain boundaries and achieving densification of ceramics. On the other hand, the smaller the particle size, the higher the interface energy, and the greater the driving force for interface diffusion. Meanwhile, the shorter distance of atom diffusion in the crystal also contributes to the rapid densification of the ceramic.

The XRD patterns of flash sintering LTTO samples are shown in Fig. 3. All samples are composed only of a tetragonal rutile phase (PDF # 21–1276), which is consistent with the structure of pure TiO_2 crystals. XRD data indicate that La^{3+} and Ta^{5+} ions have been completely solidly dissolved in the TiO_2 lattice due to relatively small doping amount. Compared with pure TiO_2 rutile phase, the (110) peak of LTTO crystal shifts toward a lower diffraction angle, as shown in Fig. 3b,

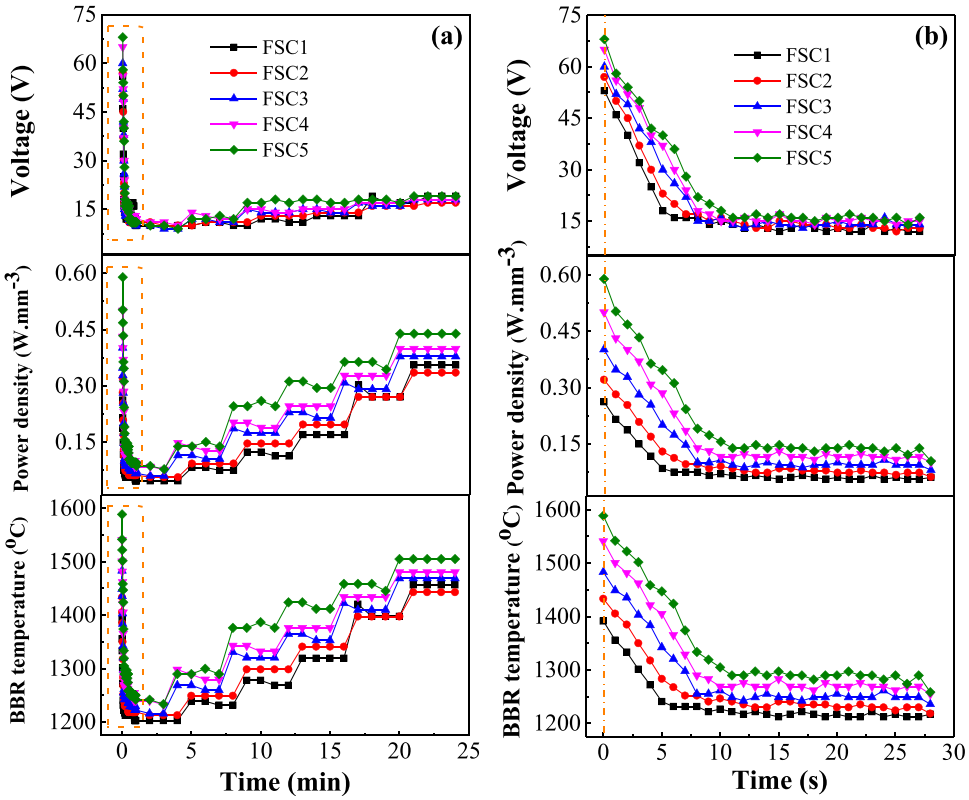

Fig. 2 Voltage, power density, and BBR temperature curve of flash sintering LTTO samples (**a**) and enlarged XRD patterns of dashed area (**b**)

Table 1 The relative density, BBR temperature, and grain size of flash sintering LTTO samples

Sample label	Green disc relative density (%)	Peak estimated temperature (^{o}C)	Grain size (μm)	FS samples relative density (%)
FSC1	58.4	1392	0.77	93.5
FSC2	58.2	1433	0.89	94.3
FSC3	57.8	1483	1.12	95.5
FSC4	58.3	1541	1.21	96.9
FSC5	58.0	1589	1.30	95.2

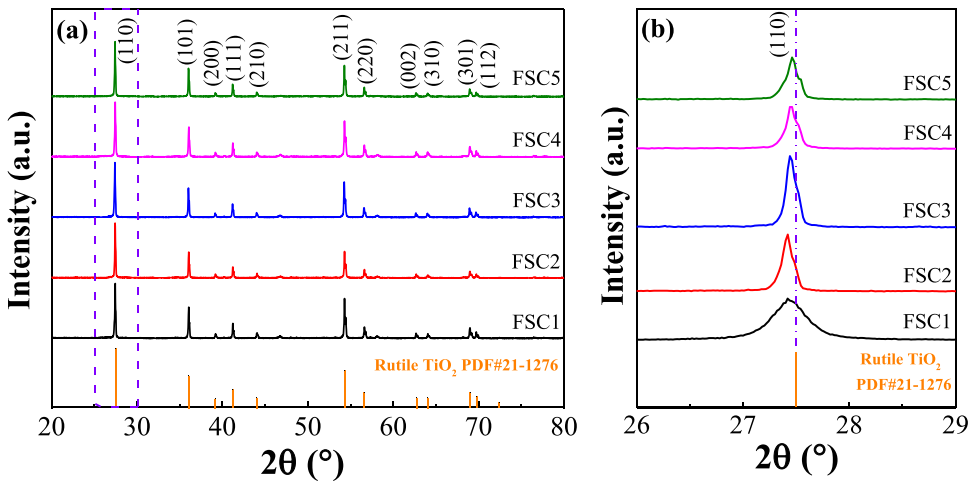

Fig. 3 XRD patterns of flash sintering LTTO samples (**a**) and enlarged XRD patterns in the range of 26°–29° (**b**)

which is attributed to the radius of doped Ta^{5+} and La^{3+} ions which is larger than that of Ti^{4+} ions, such as $r_{Ta} = 0.64$ Å, $r_{La} = 1.22$ Å, and $r_{Ti} = 0.605$ Å, respectively. With the limited current increases, the deviation of the diffraction peak gradually decreases, which may be because the high current density improves vacancy concentration, compensating for lattice distortion caused by large-sized doped ions.

Microstructure of flash sintering LTTO sample is shown in Fig. 4a–e. The grain size is small, about 1 μm, evenly distributed. This is attributed to the lower heating temperature and extremely short sintering time of flash sintering, which limits grain growth. With the limiting current rise, the grain size of flash sintering sample gradually increases, as shown in Fig. 4f. However, the relative density increased first and then decreased, with FSC4 sample having the highest relative density of 96.9%. Therefore, high density ceramics can be obtained, because the vacancy defect promotes mass transport and improves grain boundary migration during the flash sintering.

The element distribution of FSC1 sample is revealed in Fig. 5. It can be seen from the EDX spectra that the elements in the sample are only Ti, O, Ta, and La, without any impurities. Ti and O element, as the primary components, are uniformly distributed in the crystal. But Ta and La element are distributed unevenly due to the low doping concentration.

Figure. 6 represents the frequency dependence of dielectric constant (ε') and dielectric loss (tanδ) at room temperature (25 °C). All samples of La and Ta co-doped TiO_2 ceramics exhibit excellent giant dielectric constants ($\varepsilon' > 10^3$). With the improvement of test frequency, dielectric constants decrease gradually due to dielectric relaxation. At the same time, the dielectric loss is also reduced. When the limited current of flash sintering increases, dielectric constant reduces and dielectric loss increases. From the SEM measurement results in Fig. 4, the grain size becomes larger when the limited current increases. Therefore, the grain with large size reduces the grain boundary. According to the internal barrier layer capacitor (IBLC) model, the smaller the number of grain boundaries, the lower the dielectric constant. Moreover, the migration distance of charge carriers increases in large-sized grains, resulting in higher conduction losses. Obviously, LTTO ceramics can obtain the higher dielectric constant and lower dielectric loss when the limited current is small. FSC1 sample achieves excellent dielectric properties with high dielectric constant ($\varepsilon' = 7.6 \times 10^4$) and low dielectric loss (tanδ = 0.11).

Many electronic devices are used at higher temperatures, such as transportation, petrochemical, aerospace, and nuclear industries [53, 54]. Therefore, the dependence of dielectric constant and dielectric loss with temperature was measured in the range

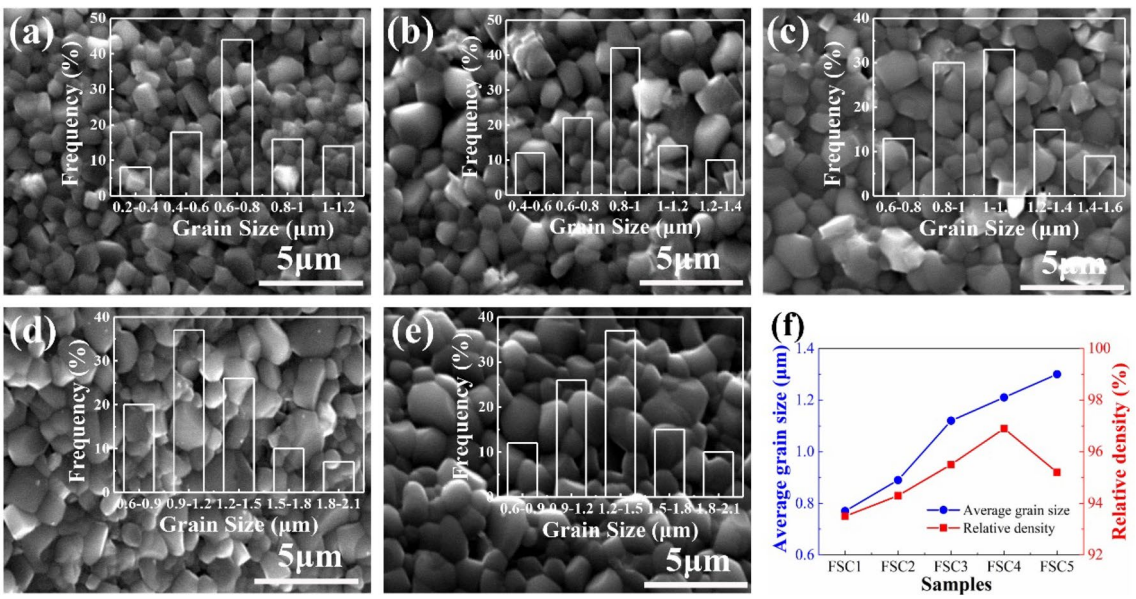

Fig. 4 SEM images of flash sintering LTTO samples **a** FSC1, **b** FSC2, **c** FSC3, **d** FSC4, **e** FSC5, **f** average grain size and relative density

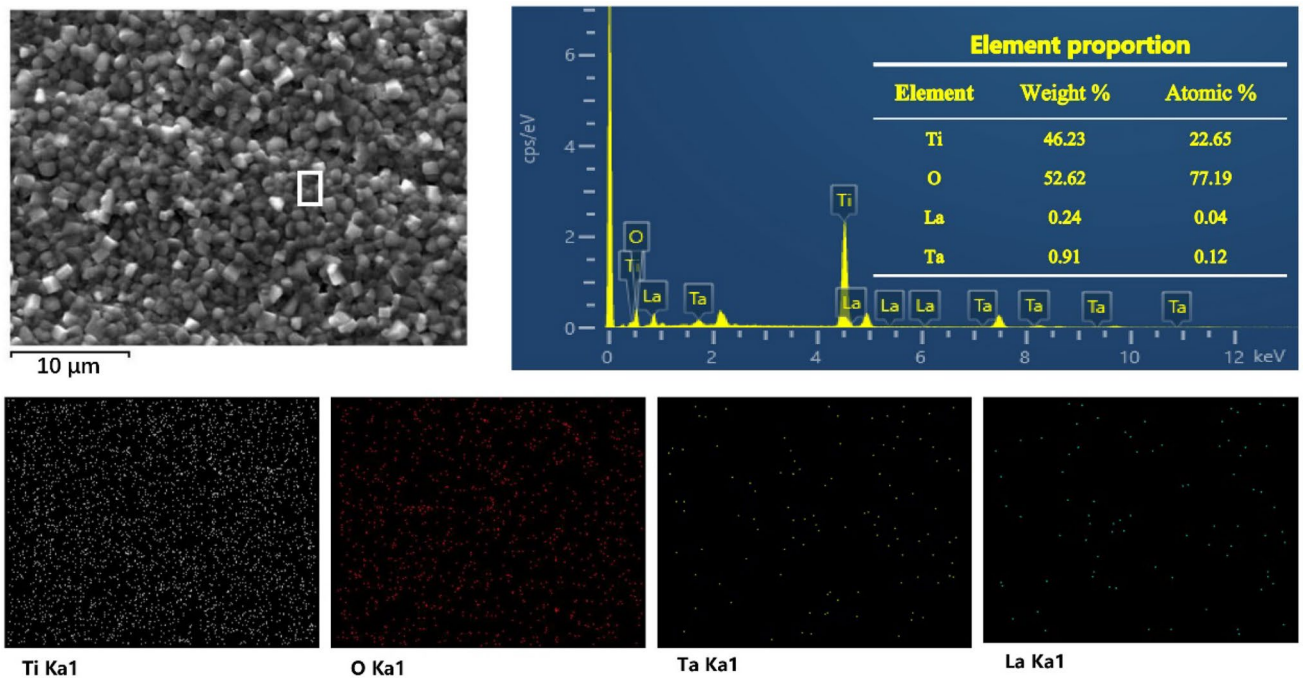

Fig. 5 The distribution of Ti, O, Ta, and La element in flash-sintered FSC1 samples

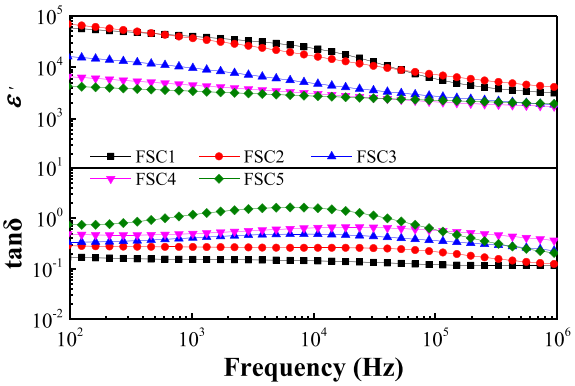

Fig. 6 Frequency dependence of dielectric properties for flash sintering LTTO samples at 30 °C

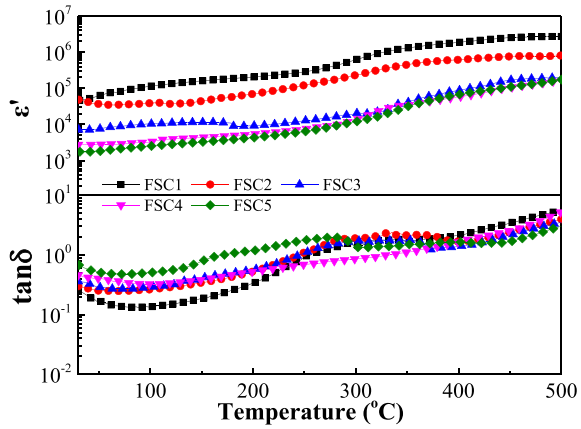

Fig. 7 Temperature dependence of dielectric properties for flash sintering LTTO samples at a frequency of 1 kHz

of 30–500 °C, as shown in Fig. 7. As the temperature rises, the dielectric constant and dielectric loss of the LTTO samples also increase. At higher the temperature, a large amount of free electrons and vacancies can be produced, and the concentration of charge carriers increases, resulting in strong dipole polarization. Meanwhile, the higher the temperature, the greater the thermal energy of the charge carriers, leading to ascend in dielectric loss. As a result, both the dielectric constant and dielectric loss increase when the temperature increases. With the increase of limited current, the large size grain reduces the number of boundaries and decreases space charge polarization, resulting in the decrease of dielectric constant and the increase of dielectric loss. It is worth noting that the dielectric loss peaks around 300 °C, which is due to changes in the polarization mechanism. At low temperature, giant dielectric constant originates from the electronic pinning defect dipole (EPDD) model. When the temperature exceeds 300 °C, free electrons with high thermal kinetic energy can break free from the binding of

defective dipoles and migrate to the grain boundary, forming the Internal Barrier Layer Capacitor (IBLC) model. At 85 oC, FSC1 sample exhibits the excellent dielectric properties, $\varepsilon' = 9.82 \times 10^4$ and tanδ = 0.13. Dielectric constant of FSC1 sample decreases gradually with increasing frequency due to dielectric relaxation [55], as shown in Fig. 8.

The nonlinear ohm characteristics represent the resistance difference of grain and grain boundary. In order to analyze the electrical properties of flash sintering LTTO ceramics, *J–E* curves of flash sintering LTTO samples are shown in Fig. 9.

When the electrical field intensity is small, the current density of samples is almost zero, and there is no change with the increase of voltage. This can be explained by the fact that grain boundaries with high resistance block the charged carrier's movement, and almost no current passes through the circuit. However, when the electric field reaches a critical value called the threshold voltage, the current density increases sharply, exhibiting significant nonlinear electrical characteristics. Moreover, the threshold voltage decreases with the increase of limited current due to the reduction of grain boundaries caused by large-sized grains. The threshold voltage (V_T), leak current (I_L), and nonlinear coefficient (α) of flash sintering LTTO samples are listed in Table 2.

Flash sintering LTTO ceramics exhibit giant dielectric properties due to the key role of doping elements. In order to investigate the oxidation states of Ti, O, Ta, and La elements, XPS testing of FSC1 samples was performed, as shown in Fig. 10. According

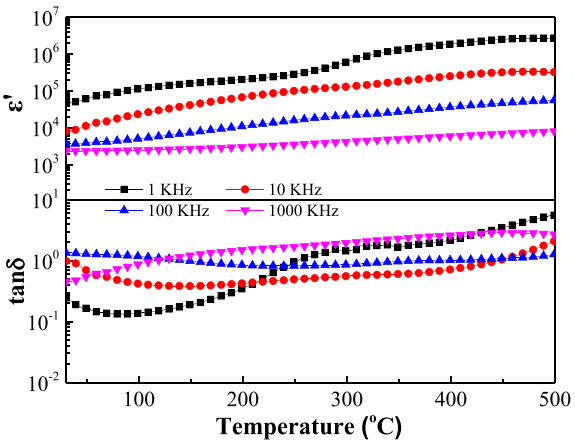

Fig. 8 Temperature dependence of dielectric properties for FSC1 sample at different frequencies

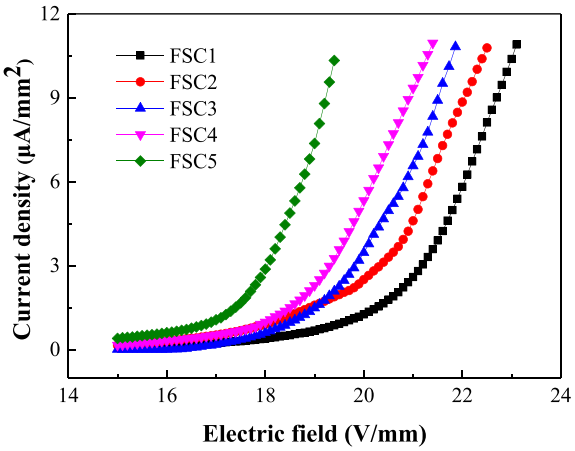

Fig. 9 The *J–E* curves of flash sintering LTTO samples

the XPS fitting results of Ta element, there are two binding energy peaks corresponding to $4f_{7/2}$ electrons at 25.2 eV and $4f_{5/2}$ electrons at 27.3 eV, respectively (see Fig. 10a). The difference in binding energy for spin orbit splitting is 2.1 eV, indicating the presence of Ta^{5+}. In Fig. 10b, the two binding energy peaks of La electrons are located at 834.9 eV and 851.7 eV, representing La $3d_{5/2}$ and La $3d_{3/2}$, respectively. At the same time, there are two companion peaks on the left side of the main peak, which are typical peak characteristics of La^{3+} in XPS spectra. Therefore, La^{3+} was confirmed in the TiO_2 lattice with a spin orbit splitting of 16.8 eV. Low priced ions (La^{3+}) replace the lattice Ti4 + to induce oxygen vacancies [56]. When La^{3+} ions, as the acceptor ion, replace Ti^{4+} ions in the lattice, oxygen vacancy defects are formed to compensate for charge balance. The defect equation is as follows:

Table 2 The threshold voltage, leak current, and nonlinear coefficient of flash sintering LTTO samples

Samples	threshold voltage[a] V_T, (V/mm)	leak current[b] I_L, (μA)	nonlinear coefficient[c] α
FSC1	20.5	279	4.7
FSC2	19.2	380	2.6
FSC3	19.5	296	3.8
FSC4	18.8	143	3.2
FSC5	17.6	516	3.5

[a]Threshold voltage at 1 mA. [b]Leakage current at 0.75 $E_{1\ mA}$. [c]$\alpha = 1/(\log E_1 - \log E_2)$, where $E_1 = 1$ mA, and $E_2 = 0.1$ mA

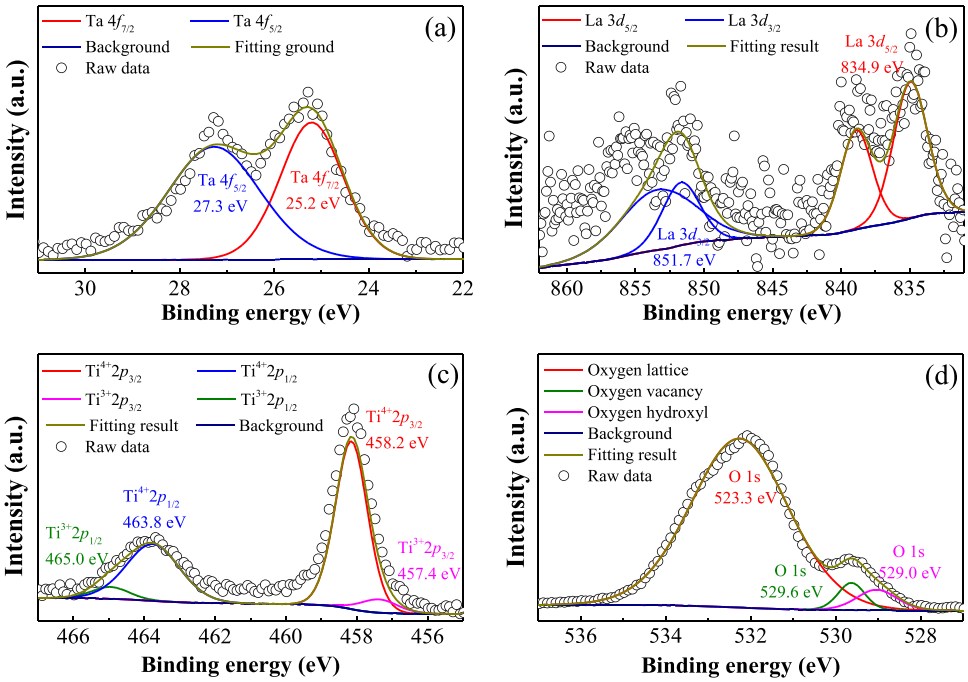

Fig. 10 The XPS spectra of FSC1 sample **a** Ti 2*p*, **b** O 1*s*, **c** Ta 4*f*, **d** La 3*d*

$$La_2O_3 \xrightarrow{2TiO_2} 2La_{Ti}' + V_O^{\cdot\cdot} + 3O_o. \quad (1)$$

As shown in Fig. 10c, the binding energies of Ti electrons exhibit two main peaks at 458.2 eV and 463.8 eV, corresponding to Ti^{4+} $2p_{3/2}$ and Ti^{4+} $2p_{1/2}$, respectively. It is worth noting that there are two small peaks located at the binding energies of 457.4 eV and 465.0 eV, representing the presence of Ti^{3+} ions. As a donor element, the doped pentavalent Ta^{5+} replaces the Ti^{4+}ion in the lattice, leaving an extra electron. The Ti^{4+}ion gains electrons and is reduced to Ti^{3+}ion, and the defect equation is as follows:

$$Ta_2O_5 + 2TiO_2 \rightarrow^{4TiO_2} 2Ta_{Ti}^{\cdot} + 2Ti_{Ti}' + 8O_o + \frac{1}{2}O_2 \uparrow \quad (2)$$

$$Ti^{4+} + e^- \rightarrow Ti^{3+}. \quad (3)$$

The binding energy of O 1*s* electrons is shown in Fig. 10d. The main peak of O 1*s* is located at 523.3 eV, representing the oxygen lattice. The other two peaks of O 1*s* represent oxygen vacancies and oxygen hydroxyl at 529.6 eV and 529.0 eV, respectively. According to Eq. (1), the concentration of oxygen vacancies depends on the doped ratio of acceptor elements (La). Oxygen vacancy is more likely to exist in the form of charge-free ($V_O^{\cdot\cdot}$) and form triangular defect complexes with other defect ions, $La_2^{3+}V_O^{\cdot\cdot}Ti^{3+}$, according to the principle of minimum system energy. Meanwhile, doped Ta^{5+} ions also form diamond-shaped defects, $Ta_2^{5+}Ti^{3+}A_{Ti}$(A=Ti^{3+}/In^{3+}/Ti^{4+}), in the same way. All defect complexes have charge interaction and form large defect clusters. Electrons are confined within clusters, forming local polarization, known as the EPDD model [29]. This is an important origin of high dielectric constant and low dielectric loss in the co-doped TiO_2 ceramics.

The resistance of the flash sintering LTTO samples was measured at 30 °C, and fitted by the ZView software through an equivalent circuit in which a capacitor is connected in parallel with a grain resistance and then connected with a grain boundary resistance, as shown in Fig. 11a. The impedance spectrum only has a portion of large semicircles arc, indicating that flash sintering LTTO samples have extremely high resistance. The nonzero intercept was found on the Z′ axis, as shown in Fig. 11b after local amplification. The intercept value represents the resistance (R_g) of semiconducting grains, indicating a lower resistance inside the grains. The grain resistance gradually decreases with the increase of the limited current of the sample, which is attributed to a large number of charge carriers by the high limited current during flash sintering. The diameter of the semi-circular arc represents the total resistance value (R_{bulk}) of the sample, which is too high to be fully displayed. The resistance difference of

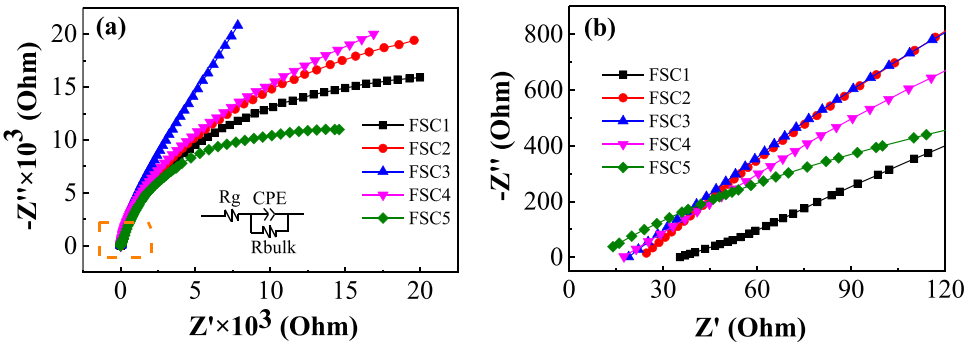

Fig. 11 Room-temperature impedance spectra of flash sintering LTTO ceramics (**a**) and enlarged views closed to the origin (**b**)

grain and sample is the resistance of grain boundary (R_{gb}). Therefore, LTTO samples are composed of grains with low resistance and grain boundaries with extremely high resistance, i.e., $R_{gb} >> R_g$. The charge carrier accumulates at the edge of insulating grain boundary by the action of applied electric field, resulting in interface polarization, which is called the internal barrier layer capacitor model (IBLC) [30, 57]. As a result, interface polarization is an important reason of giant dielectric constant for flash sintering LTTO samples.

4 Conclusion

$(La_{1/2}, Ta_{1/2})_{0.02}Ti_{0.98}O_2$ ceramics were prepared by flash sintering technology at 1100 °C for 24 min. Under the different limited current, LTTO sample only have rutile phase, without any second phase. With the increase of limited current, the grain size also increases, but the relative density first increases and then decreases. The highest relative density of FSC4 samples is 96.9%, which is close to full densification ceramics. At 30 °C, FSC1 samples with small-sized grains exhibit the best dielectric properties, $\varepsilon' = 7.6 \times 10^4$ and $\tan\delta = 0.11$. As the testing temperature increases, both the dielectric constant and dielectric loss of the sample increase. At 85 oC and 1 kHz, the dielectric loss of FSC1 sample is only 0.13, while dielectric constant reaches 9.82×10^4. At lower temperatures, the giant dielectric constant of samples originates from the EPDD model, in which the doped donor ions (Ta^{5+}) and acceptor ions (La^{3+}) form defect complex clusters, resulting in local polarization. As the temperature increases, the IBLC model plays an important role in the giant dielectric constant of flash sintering LTTO samples, which is attributed to the accumulation of charge carriers at insulating grain boundaries with extremely high resistance, resulting in interface polarization. As a result, the giant dielectric properties of co-doped TiO_2 ceramics are attributed to the co-action of EPDD and IBLC model. By flash sintering, LTTO samples can be rapidly densified in a short sintering time and exhibit excellent giant dielectric properties.

Acknowledgements

This work was financially supported by National Natural Science Foundation of China (Grant No. 52072004), Key Scientific Research Project of University in Anhui Province (2023AH040124), and Key Research and Development and Achievement Transformation Project of Science and Technology Projects in Wuhu City (2023yf032).

Author contributions

ZY: Methodology, Design, Investigation, Preparation, Writing. XW: Experiment, Investigation. LZ: Experiment, Analyzing. HL: Investigation, Guiding. HZ: Analyzing, Data curation. DX: Conceptualization, Guiding, Review, Supervision. All authors read the paper and commented on the text.

Data availability

The authors declare that they have no known competing financial interests or personal relationships that could have appeared to influence the work reported in this paper. The data that support the findings of this study are available from the corresponding author upon reasonable request.

References

1. X. Zhao, N. Yan, Y. Li, Z. Shen, R. Huang, C. Xu, X. Zhao, X. Wang, R. Zhang, Z. Jia, Dielectric barrier discharge-based defect engineering method to assist flash sintering. J. Adv. Ceram. **12**, 1046–1057 (2023)
2. J. Yang, L. Tan, P. Ji, F. Sun, Q. Tian, X. Su, Rapid preparation of $Gd_2Zr_{2-x}Ce_xO_7$ waste forms by flash sintering and their chemical durability. J. Eur. Ceram. Soc. **43**, 4950–4957 (2023)
3. C. Shen, T. Niu, B. Yang, J. Cho, Z. Shang, T. Sun, A. Shang, R. Edwin García, H. Wang, X. Zhang, Micromechanical properties and microstructures of AC and DC flash-sintered alumina. Mat. Sci. Eng. A **866**, 144631–144640 (2023)
4. M. Cologna, B. Rashkova, R. Raj, Flash Sintering of Nanograin Zirconia in <5 s at 850 °C. J. Am. Ceram. Soc. **93**, 3556–3559 (2010)
5. Z. Yan, A. Wu, X. Wang, R. Huang, N. Yan, Z. Jia, L. Wang, ZnO as sintering aid and reactant for reactive flash sintering at room temperature. Ceram. Int. **48**, 21037–21042 (2022)
6. G. Zhao, S. Cai, Y. Zhang, H. Gu, C. Xu, Reactive flash sintering of high-entropy oxide (La0.2Nd0.2Sm0.2Eu0.2Gd0.2)2Zr2O7: Microstructural evolution and aqueous durability. J. Eur. Ceram. Soc. **43**, 2593–2600 (2023)
7. S. Yang, P. Wei, R. Pang, L. Fan, X. Fu, L. An, Effects of doping cations on the densification and microstructure of flash-sintered α-Al_2O_3. J. Eur. Ceram. Soc. **43**, 2045–2050 (2023)
8. J. Yang, M. Fu, Q. Tian, L. Meng, L. Zhang, Y. Liu, J. Xie, X. Su, J. Peng, Preparation of $Gd_2Zr_2O_7$ nanoceramics by flash sintering and two-step flash sintering. Ceram. Int. **49**, 16594–16602 (2023)
9. W. Rheinheimer, X.L. Phuah, L. Porz, M. Scherer, J. Cho, H. Wang, The impact of flash sintering on densification and plasticity of strontium titanate: high heating rates, dislocation nucleation and plastic flow. J. Eur. Ceram. Soc. **43**, 3524–3537 (2023)
10. A. Nakamoto, K. Nambu, H. Masuda, H. Yoshida, Chemical bonding and crystal structure in flash sintered Y_2O_3 under DC or AC field. J. Eur. Ceram. Soc. **43**, 3516–3523 (2023)
11. I. Mazo, B. Palmieri, A. Martone, M. Giordano, V.M. Sglavo, Flash sintering in metallic ceramics: finite element analysis of thermal runaway in tungsten carbide green bodies. J. Mater. Res. Technol. **23**, 5993–6004 (2023)
12. Y. Li, C. Xu, R. Huang, X. Zhao, X. Wang, Z. Jia, Mechanism analysis of arc-induced flash sintering of 3YSZ at room temperature. J. Eur. Ceram. Soc. **43**, 7033–7040 (2023)
13. M. Li, D. Wu, Y. Zhu, L. Guan, Y. Huang, X. Song, Low-temperature preparation of $La_{0.9}Ca_{0.1}CrO_3$ semiconductor ceramics by flash sintering. Ceram. Int. **49**, 29364–29369 (2023)
14. X.L. Phuah, B. Yang, H. Charalambous, T. Tsakalakos, X. Zhang, H. Wang, Microstructure and defect gradients in DC and AC flash sintered ZnO. Ceram. Int. **47**, 28596–28602 (2021)
15. A. Alvarez, Y. Dong, I.-W. Chen, DC electrical degradation of YSZ: Voltage-controlled electrical metallization of a fast ion conducting insulator. J. Am. Ceram. Soc. **103**, 3178–3193 (2020)
16. X. Wang, Y. Zhu, R. Huang, H. Mei, Z. Jia, Flash sintering of ZnO ceramics at 50 °C under an AC field. Ceram. Int. **45**, 24909–24913 (2019)
17. M. Yu, S.E. Grasso, R. Mckinnon, T. Saunders, M.J. Reece, Review of flash sintering: materials, mechanisms and modelling. Adv. Appl. Ceram. **116**, 24–60 (2016)
18. A. Eqbal, K.S. Arya, T. Chakrabarti, In-depth study of the evolving thermal runaway and thermal gradient in the dog bone sample during flash sintering using finite element analysis. Ceram. Int. **46**, 10370–10378 (2020)
19. A. Eqbal, T. Chakrabarti, Study on the electrochemical effect of ZnO addition on flash sintering of 3 mol% yttria stabilized zirconia. J. Eur. Ceram. Soc. **43**, 6260–6271 (2023)
20. R. Raj, Joule heating during flash sintering. J. Eur. Ceram. Soc. **32**, 2293–2301 (2012)
21. R. Serrazina, P.M. Vilarinho, A.M.O.R. Senos, L. Pereira, I.M. Reaney, J.S. Dean, Modelling the particle contact influence on the Joule heating and temperature distribution during flash sintering. J. Eur. Ceram. Soc. **40**, 1205–1211 (2020)
22. S. Bhandari, T.P. Mishra, O. Guillon, D. Yadav, M. Bram, Accessing the role of Joule heating on densification during flash sintering of YSZ. Scripta Mater. **211**, 114508–114514 (2022)
23. R. Chaim, Particle surface softening as universal behaviour during flash sintering of oxide nano-powders. Materials (Basel) **10**, 179–188 (2017)
24. R. Raj, M. Cologna, J.S.C. Francis, Influence of externally imposed and internally generated electrical fields on grain growth, diffusional creep, sintering and related phenomena in ceramics. J. Am. Ceram. Soc. **94**, 1941–1965 (2011)
25. J. Janek, C. Korte, Electrochemical blackening of yttria-stabilized zirconia-morphological instability of the moving reaction front. Solid State Ionics **116**, 181–195 (1999)

26. Y. Zhang, J. Nie, J.M. Chan, J. Luo, Probing the densification mechanisms during flash sintering of ZnO. Acta Mater. **125**, 465–475 (2017)
27. J. Narayan, A new mechanism for field-assisted processing and flash sintering of materials. Scripta Mater **69**, 107–111 (2013)
28. M.Z. Becker, N. Shomrat, Y. Tsur, Recent advances in mechanism research and methods for electric-field-assisted sintering of ceramics. Adv. Mater. **30**, 1706369–1706376 (2018)
29. W. Hu, Y. Liu, R.L. Withers, T.J. Frankcombe, L. Norén, A. Snashall, M. Kitchin, P. Smith, B. Gong, H. Chen, J. Schiemer, F. Brink, J.W. Leung, Electron-pinned defect-dipoles for high-performance colossal permittivity materials. Nat. Mater. **12**, 821–826 (2013)
30. L. Zhou, Z. Peng, J. Zhu, Q. Shi, P. Liang, L. Wei, D. Wu, X. Chao, Z. Yang, High temperature stability and low dielectric loss in colossal permittivity TiO2 based ceramics co-doped with Ag+ and Mo6+. Mater. Chem. Phys. **295**, 127072–127080 (2023)
31. N. Thanamoon, N. Chanlek, P. Srepusharawoot, P. Moontragoon, P. Thongbai, Giant dielectric properties of terbium and niobium co-doped TiO_2 ceramics driven by intrinsic and extrinsic effects. J. Alloy. Compd. **935**, 168095–168103 (2023)
32. N. Thongyong, N. Chanlek, P. Srepusharawoot, M. Takesada, D.P. Cann, P. Thongbai, Experimental study and DFT calculations of improved giant dielectric properties of Ni^{2+}/Ta^{5+} co-doped TiO_2 by engineering defects and internal interfaces. J. Eur. Ceram. Soc. **42**, 4944–4952 (2022)
33. N. Thanamoon, N. Chanlek, P. Moontragoon, P. Srepusharawoot, P. Thongbai, Microstructure, low loss tangent, and excellent temperature stability of Tb+Sb-doped TiO_2 with high dielectric permittivity. Results Phys. **37**, 105536–105546 (2022)
34. J. Zhu, D. Wu, P. Liang, X. Zhou, Z. Peng, X. Chao, Z. Yang, Ag^{+}/W^{6+} co-doped TiO_2 ceramic with colossal permittivity and low loss. J. Alloy. Compd. **856**, 157350–157358 (2021)
35. P. Liang, J. Zhu, D. Wu, H. Peng, X. Chao, Z. Yang, Good dielectric performance and broadband dielectric polarization in Ag, Nb co-doped TiO_2. J. Am. Ceram. Soc. **104**, 2702–2710 (2021)
36. J. Fan, T. Yang, Z. Cao, Colossal permittivity and multiple effects in (Zn+Ta) codoped TiO_2 ceramics. J. Asian Ceram. Soc. **8**, 1188–1196 (2020)
37. J. Liu, L. Wang, X. Yin, Q. Yua, D. Xu, Effect of ionic radius on colossal permittivity properties of (A, Ta) co-doped TiO_2 (A=alkaline-earth ions) ceramics. Ceram. Int. **46**, 12059–12066 (2020)
38. X. Zhao, L. Chen, X. Zhang, P. Liu, C. Xu, Z. Hou, Z. Wang, F. Wang, J. Wang, G. Shi, The abnormal multiple dielectric relaxation responses of Al^{3+} and Nb^{5+} co-doped rutile TiO_2 ceramics. J. Alloy. Compd. **860**, 157891–157898 (2021)
39. W. Tuichai, S. Danwittayakul, J. Manyam, N. Chanlek, M. Takesada, P. Thongbai, Giant dielectric properties of Ga^{3+}-Nb^{5+} Co-doped TiO_2 ceramics driven by the internal barrier layer capacitor effect. Materials **18**, 101175–101188 (2021)
40. M. Wang, J. Xie, K. Xue, L. Li, Effects of Eu3+/Ta5+ non-stoichiometric ratio on dielectric properties of (EuxTa1-x)0.08Ti0.92O2 ceramics with colossal permittivity: experiments and first-principal calculations. Ceram. Int. **47**, 24868–24876 (2021)
41. Y. Mingmuang, N. Chanlek, P. Thongbai, Ultra-low loss tangent and giant dielectric permittivity with excellent temperature stability of TiO_2 co-doped with isovalent-Zr^{4+}/pentavalent-Ta^{5+} ions. J. Materiomics **6**, 1269–1277 (2022)
42. Y. Mingmuang, N. Chanlek, P. Moontragoon, P. Srepusharawoot, P. Thongbai, Effects of Sn4+ and Ta5+ dopant concentration on dielectric and electrical properties of TiO_2: internal barrier layer capacitor effect. Results Phys. **42**, 106029–106037 (2022)
43. J. Liu, J. Xu, B. Cui, Q. Yu, S. Zhong, L. Zhang, S. Du, D. Xu, Colossal permittivity characteristics and mechanism of (Sr, Ta) co-doped TiO_2 ceramics. J. Mater. Sci-Mater. El. **31**, 5205–5213 (2020)
44. X. Guo, J. Kang, R. Gu, H. Hao, Y. Tang, L. Jin, X. Wei, Enhanced dielectric performance of Niobium and Thulium modified rutile TiO_2 ceramics by defect regulation. Ceram. Int. **49**, 14804–14811 (2023)
45. Y. Meng, K. Liu, X. Zhang, X. Lei, J. Chen, Z. Yang, B. Peng, C. Long, L. Liu, C. Li, Defect engineering in rare-earth-doped $BaTiO_3$ ceramics: route to high-temperature stability of colossal permittivity. J. Am. Ceram. Soc. **105**, 5725–5737 (2022)
46. Y. Mingmuang, N. Chanlek, P. Moontragoon, P. Srepusharawoot, P. Thongbai, significantly improved dielectric properties of tin and niobium co-doped rutile TiO_2 driven by Maxwell-Wagner polarization. J. Alloy. Compd. **923**, 166371–166380 (2022)
47. C. Chen, Y. Xie, P. Chen, C. Wang, Mechanisms of the relaxations in (In+Nb) co-doped TiO_2 ceramics. Ceram. Int. **47**, 26019–26024 (2021)
48. P. Peng, C. Chen, B. Cui, J. Li, D. Xu, B. Tang, Influence of the electric field on flash-sintered (Zr + Ta) co-doped TiO_2 colossal permittivity ceramics. Ceram. Int. **48**, 6016–6023 (2022)

49. Z. Wang, P. Peng, L. Zhang, N. Wang, B. Tang, B. Cui, J. Liu, D. Xu, Effect of electric field on the microstructure and electrical properties of (In + Ta) co-doped TiO_2 colossal dielectric ceramics. J. Mater. Sci-Mater. El. **33**, 6283–6293 (2022)
50. Z. Yang, P. Wang, Z. Wang, J. Liu, L. Zhang, S. Zhong, B. Tang, D. Xu, Controllable low-temperature flash sintering and giant dielectric performance of (Zn, Ta) co-doped TiO2 ceramics. Ceram. Int. **48**, 24629–24637 (2022)
51. Z. Wang, M. Shi, J. Liu, J. Li, L. Zhang, Z. Cheng, J. Qin, Y. Jiu, B. Tang, D. Xu, Flash sintering preparation and colossal dielectric origin of $(Al_{0.5}Ta_{0.5})_{0.05}Ti_{0.95}O_2$ ceramics. J. Mater. Sci.-Mater. El. **33**, 15802–11583 (2022)
52. Y. Mei, S. Pandey, W. Long, J. Liu, S. Zhong, L. Zhang, S. Du, D. Xu, Processing and characterizations of flash sintered ZnO-Bi_2O_3-MnO_2 varistor ceramics under different electric fields. J. Eur. Ceram. Soc. **40**, 1330–1337 (2020)
53. Z. Liu, H. Fan, S. Lei, X. Ren, C., Long, Duplex structure in $K_{0.5}Na_{0.5}NbO_3$-$SrZrO_3$ ceramics with temperature-stable dielectric properties. J. Eur. Ceram. Soc. **37**, 115–122 (2017)
54. J. Shi, H. Fan, X. Liu, Y. Ma, Q. Li, Bi deficiencies induced high permittivity in lead-free BNBT-BST high-temperature dielectrics. J. Alloy. Compd. **627**, 463–467 (2015)
55. K. Tsuji, H. Han, S. Guillemet-Fritsch, C.A. Randal, Dielectric relaxation and localized electron hopping in colossal dielectric (Nb, In)-doped TiO_2 rutile nanoceramics. Phys. Chem. Chem. Phys. **19**, 8568–8574 (2017)
56. X. Liu, H. Fan, J. Shi, Q. Li, Origin of anomalous giant dielectric performance in novel perovskite: Bi0.5-xLaxNa0.5-xLixTi1-yMyO3 (M = Mg2+, Ga3+). Sci. Rep. **5**, 12699–12709 (2015)
57. N. Thanamoon, N. Chanlek, P. Srepusharawoot, P. Thongbai, Origin of colossal dielectric performance of rutile-TiO_2 by substitution with Y^{3+}+Ta^{5+} dopants: DFT calculations and experimental study. Materials **22**, 101432–101442 (2022)